Effect of deprotonation on absorption and emission spectra of Ru(II)-bpy complexes functionalized with carboxyl groups†

Ekaterina Badaeva,[bc] Victor V. Albert,[ab] Svetlana Kilina,[b] Alexey Koposov,[d] Milan Sykora[d] and Sergei Tretiak*[b]

Received 26th November 2009, Accepted 12th April 2010
DOI: 10.1039/b924910a

Changes in the ground and excited state electronic structure of the $[Ru(bpy)_3]^{2+}$ (bpy = 2,2′-bipyridine) complex induced by functionalization of bpy ligands with carboxyl and methyl groups in their protonated and deprotonated forms are studied experimentally using absorption and emission spectroscopy and theoretically using density functional theory (DFT) and time dependent DFT (TDDFT). The introduction of the carboxyl groups shifts the metal-to-ligand-charge-transfer (MLCT) absorption and emission bands to lower energies in functionalized complexes. Our calculations show that this red-shift is due to the stabilization of the lowest unoccupied orbitals localized on the substituted ligands, while the energies of the highest occupied orbitals localized on the Ru-center are not significantly affected. Consistent with previously observed trends in optical spectra of related Ru(II) complexes, deprotonation of the carboxyl groups results in a blue shift in the absorption and phosphorescence spectra. The effect originates from interplay of positive and negative solvatochromism in the protonated and deprotonated complexes, respectively. This results in more delocalized character of the electron transition orbitals in the deprotonated species and a strong destabilization of the three lowest unoccupied orbitals localized on the substituted and unsubstituted ligands, all of which contribute to the lowest-energy optical transitions. We also found that owing to the complexity of the excited state potential energy surfaces, the calculated lowest triplet excited state can be either weakly optically allowed ^{3}MLCT or optically forbidden Ru ^{3}d–d transition depending on the initial wavefunction guess used in TDDFT calculations.

Introduction

Polypyridine complexes of Ruthenium (II) are among the most studied compounds in coordination chemistry.[1–3] Their unique combination of chemical stability, strong visible absorption and emission, excited state reactivity, and redox and catalytic properties has stimulated efforts to exploit these compounds in artificial photosynthesis,[4] molecular electronics,[5] light emitting devices,[6] electroluminescent detectors and sensors,[7] biological and medical diagnostics,[8] *etc*.

One of the features of Ru(II)-polypyridine complexes, particularly appealing for solar energy conversion applications, is that their chemical reactivity and electronic properties can be tuned *via* modifications of peripheral ligands.[2] For example, in TiO_2-based photovoltaic devices (Grätzel cells), where Ru(II)-polypyridine complexes are typically used as sensitizers, the bipyridyl ligands are modified with one or more carboxylic[9,10] or phosphonic[11] acid functionalities to provide means for chemical and electronic coupling of the complexes to the semiconductor surface. Modification of the non-anchoring ligands is also commonly used in order to tailor the absorption spectra of the complexes to maximize their ability to harvest the solar radiation.[12,13] In a device, the absorption of a photon by the chemically and electronically optimized complex is followed by a rapid electron transfer from its excited state into the conduction band of TiO_2. This provides a basis for conversion of solar radiation into electrical current. Meyer and coworkers have demonstrated[14,15] that in appropriately modified Ru(II) complexes, the oxidizing equivalents stored in the complex following the electron injection into TiO_2 can be also used to drive chemical processes such as catalytic oxidation of organic substrates. Such TiO_2-complex assemblies can serve as a basis for solar-to-chemical energy conversion devices. Recently, an alternative approach has been proposed based on chemical coupling of Ru(II)-polypyridine complexes with CdSe semiconductor quantum dots.[16]

An important aspect of the chemical coupling of the complexes to semiconductors *via* carboxylic acid functional groups is that the anchoring group is typically deprotonated, which leads to changes in the electronic structure of the complexes.[17–19] Such a change can have a significant impact

[a] *Quantum Theory Project, Departments of Chemistry and Physics, University of Florida, Gainesville FL 32611, USA. E-mail: serg@lanl.gov, skilina@gmail.com*
[b] *Theoretical Division, Center for Nonlinear Studies (CNLS), and Center for Integrated Nanotechnologies (CINT), Los Alamos National Laboratory, USA*
[c] *University of Washington, Seattle, WA 98195, USA*
[d] *Chemistry Division, C-PCS, Los Alamos National Laboratory, Los Alamos, NM 87545, USA*
† Electronic supplementary information (ESI) available: Supplementary Fig. S1–S10. See DOI: 10.1039/b924910a

on the optical spectra and redox properties of the complexes and ultimately on the the overall performance of a solar energy conversion device. To better understand the effect of deprotonation on the electronic structure and optical spectra, several computational studies based on density functional theory (DFT) and time dependent DFT (TDDFT) were recently carried out on a series of Ru(II)-polypyridine complexes derivatized with protonated and deprotonated form of the carboxylic acid in different solvents.[20–24] In these studies, the focus was on the thiocyanate derivatives, such as $[Ru(4,4'\text{-}COOH\text{-}2,2'\text{-}bpy)_2(NCS)_2]$ and related complexes, which are commonly used as sensitizers in the TiO_2-based solar cells.[25] Experimental and theoretical studies of these compounds revealed that the blue shift of the absorption onset caused by deprotonation of carboxyl groups is induced by destabilization of the lowest unoccupied molecular orbital (LUMO).[23,24] The pathways of radiative relaxation in the Ru-polypyridine complexes have been intensively studied experimentally[18,26–28] and theoretically.[20,29–33] These studies showed that the excited state potential energy surfaces are very complex in these molecules. In particular, the triplet state dynamics[34,35] and emission (phosphorescence) is found to be very efficient in these complexes due to the the lower lying triplet metal-to-ligand charge transfer state (^{3}MLCT) or the triplet ligand $\pi \rightarrow \pi^*$ state. The nature of the lowest triplet state and the emission energy depend on experimental conditions, such as solvent polarity, pH, type of the counterions, as well as on the structure of the ligands and degree of protonation of ligand functional groups.[36–38]

Here, we present joint experimental and theoretical (DFT and TDDFT) studies of absorbing and emitting states for a family of related, but previously not studied complexes with the general form of $[Ru(bpy)_x(L)_{3-x}]^{2+}$, where L = 4-carboxy-4′-methyl-2,2′-bipyridine or 4,4′-dicarboxy-2,2′-bipyridine. Our interest in these systems mostly stems from recent experiments, where these complexes have been used to model and study charge transfer processes between the complex and CdSe quantum dots in the context of potential applications of these materials for photocatalysis.[16] We specifically focus on the effects of the carboxyl group position and its deprotonation on the electronic structure and optical spectra of these complexes. We also investigate possible mechanisms of phosphorescence and triplet state ordering in these molecules. General absorption and emission trends consistent with previous studies of related compounds,[22–24,31,32,39] are observed. To rationalize these trends, we calculate and analyze the singlet and triplet excited state natural transition orbitals (NTOs) derived from TDDFT results and compare them with the ground state molecular orbitals (MOs) obtained by DFT calculations.

Methods and computational details

We study ground and excited state properties of four Ru(II)-bipyridine complexes with the general structure $[Ru(bpy)_x(L)_{3-x}]^{2+}$. The structure where $x = 3$ corresponds to tris(2,2′-bipyridine) Ru(II), $[Ru(bpy)_3]^{2+}$, denoted here as complex **1**. The complexes with $x = 2$ and L = 4-carboxy-4′-methyl-2,2′-bipyridine (mcb) or L = 4,4′-dicarboxy-2,2′-bipyridine (ccb) are referred to as **2** and **4**, respectively. The complex with $x = 1$ and L = mcb is labeled in our paper as **3**. The fully deprotonated forms (denoted as **2a**, **3a**, and **4a**) of complexes **2–4**, respectively, are also studied both theoretically and experimentally. Schematic chemical structures of all complexes under investigation are presented in Fig. 1.

All calculations, including ground state geometry optimization and excited state electronic structure modeling, were performed using Gaussian09 and Gaussian03 program suites[40] which allow calculation of natural transition orbitals (NTOs).[41] The geometries of the molecules were optimized both for the ground state (closed-shell singlet S_0) and the lowest-energy excited singlet (^{1}MLCT) or triplet state (either ^{3}MLCT or ^{3}d–d), see Fig. 2. All procedures of geometry optimization were done at the DFT level of theory implementing the hybrid B3LYP functional[42] and solvent effects. The LANL2DZ basis set was chosen for the heavier Ru atom, while the remaining atoms were modeled with the 6-31G* basis set.

The chosen method represents one of the currently most popular DFT functionals and basis sets, which previously has shown good agreement with uv-vis experimental data for various Ru(II) complexes.[32,43–46] The validity of various DFT functionals for description of geometry and optical properties of various transition metal complexes have already been tested many times. For series of Ruthenium, Osmium, and Lanthanide complexes, excited states energies and electron distributions have been found to be dependent on the amount of Hartree–Fock exchange[47] and are well reproduced by the hybrid DFT functionals, such as B3LYP,[20,23,48,49] while semi-local DFT functionals, such as PBE and PW91, usually result in a significant red shift of calculated spectra compared to experimental data.[22] For example, Gorelsky *et al.*[50] have compared TDDFT calculations of optical spectra of $Ru(NH_3)$(bpy) complexes performed with different functionals and basis sets. They concluded that B3LYP functional usually gives the best results both for optimal geometries and electronic spectra. For broader picture on performance of different DFT functionals when applied to transition metal complexes, we refer the reader to the recent reviews.[51,52]

Solvent effects in all studied Ru(II) complexes were simulated by embedding the molecule in a polarizable continuum medium (PCM) with an appropriate dielectric constant. Here we chose PCM that performs a reaction field calculation using the integral equation formalism model (IEFPCM),[53,54] as implemented in Gaussian09 and Gaussian03. Acetonitrile (CH_3CN, $\varepsilon = 35.688$) was chosen as a reference solvent for consistency with the experimental studies.[16] Solvent implementation in Gaussian09 is expected to be more advanced compared to Gaussian03 since it provides better continuity, smoothness and robustness of the reaction field with respect to atomic positions and external perturbing fields.[55] For example, PCM-Gaussian09 model we use here builds up the cavity by placing a sphere around each solute atom, including hydrogens. In contrast, PCM-Gaussian03 model places a sphere only around heavy atoms, so that hydrogens are enclosed in the sphere of the heavy atom to which they are bonded. Nonetheless, solvent medium calculations are highly

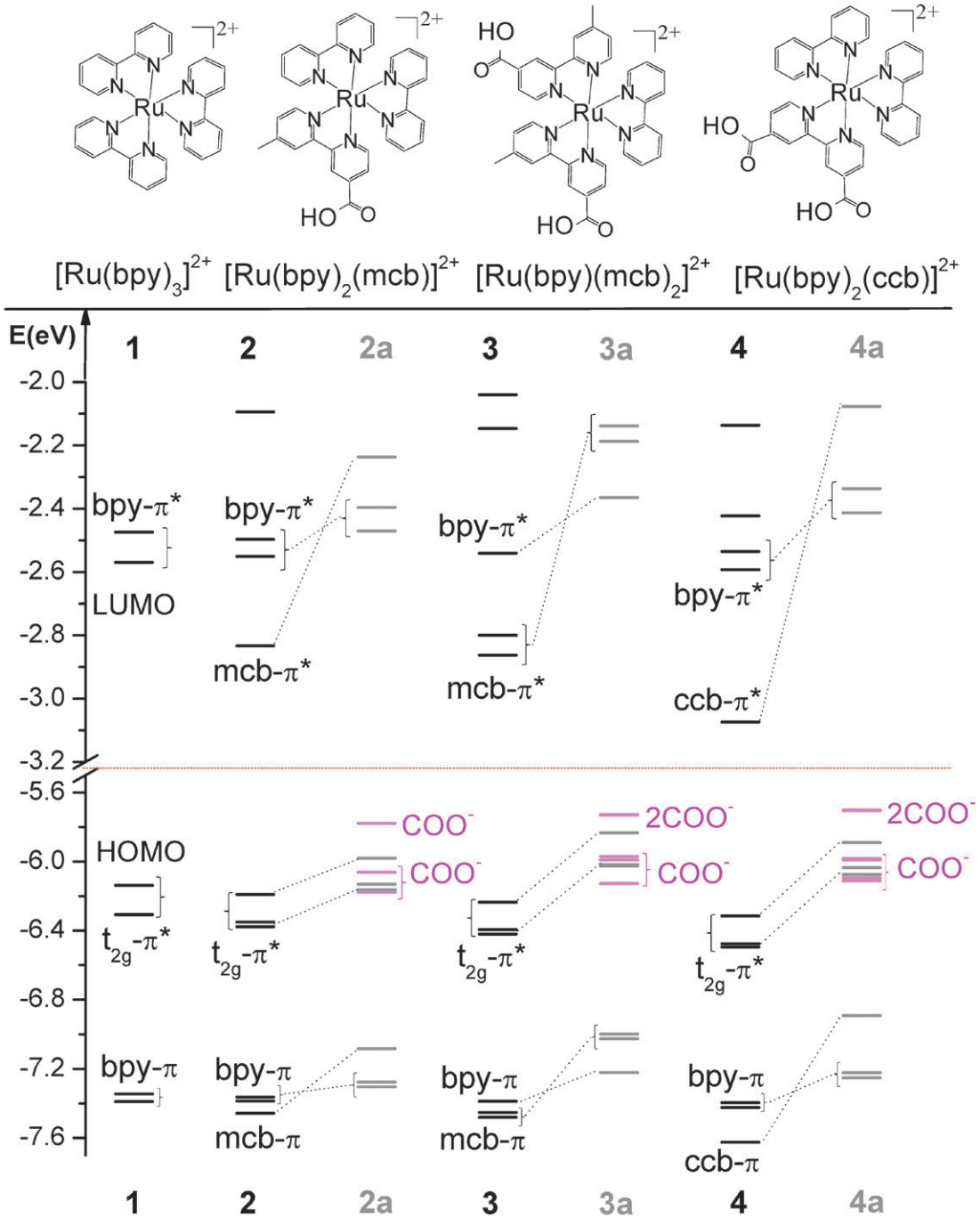

Fig. 1 Chemical structures and calculated molecular orbital (MO) levels (eV) of the studied Ru(II)-polypiridine complexes. The electronic structures (grey lines) defined by **2a**, **3a**, and **4a** correspond to the fully deprotonated derivatives of the complexes **2**, **3**, and **4**, respectively.

parametrized; therefore, it is useful to have an experimental reference to which modeling choices can be validated in each calculation.

As was previously found, inclusion of the solvent into calculations of the excited states of Ru(II) complexes is very important.[22,24,33,39,44] In our case, addition of solvent led to a better agreement between theory and experiment. Solvent implementation appeared to be crucial for the description of excitations in the deprotonated complexes through removing the nonphysical charge-transfer (CT) states away from the optical gap. We also found that the solvation model strongly impacts the ground state electronic structure, especially in the deprotonated complexes. This effect has not been addressed in the previous studies. Therefore, here we analyze in detail the effect of different PCM solvation models implemented in GAUSSIAN03 and GAUSSIAN09 on the ground state electronic structure of the complexes **2a**–**4a**, optimized in both vacuum and acetonitrile.

The excited states were studied using linear response TDDFT formalism with the same functional and basis set as

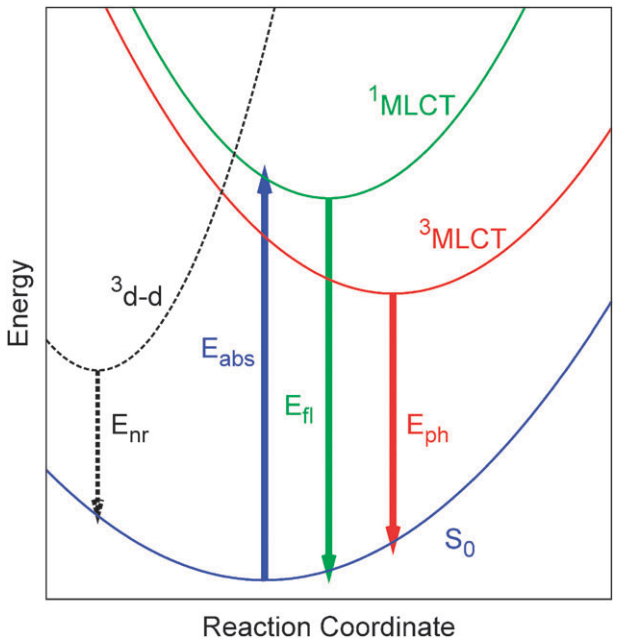

Fig. 2 Schematic representation of potential energy surfaces for main types of electronic levels in the studied complexes, including ground S_0 and ^{1}MLCT singlet as well as ^{3}MLCT and ^{3}d–d triplet states. Arrows show transition energies for absorption (E_{abs}), fluorescence (E_{fl}), and phosphorescence (E_{ph}) processes. Several higher lying ^{1}MLCT states (not shown) are particularly active in absorption and form spectral bands I and II. Evolution on ^{3}d–d surface results in non-rediative decay.

described above. Advanced PCM-Gaussian09 solvation model was used to analyze solvent effects. The energetics of essential electronic states is shown in Fig. 2. For the absorption spectra of protonated complexes, 50 lowest singlet transitions were calculated to reach the transition energies up to 4.5 eV. For deprotonated species, up to 80 singlet excitations had to be taken into account to cover the same energy range. These TDDFT solutions provided vertical excitation energies at the ground state optimal geometry appearing as peaks in the absorption spectra. The latter were modeled by broadening each spectral line obtained from TDDFT calculations (*i.e.*, oscillator strength at the respective excitation energy) by a Gaussian function with a linewidth of 0.1 eV to match the experimentally observed absorption lineshapes.

The molecular emission energy originating from the singlet states (fluorescence) has been calculated as a vertical transition energy of the lowest singlet excited state at its optimal geometry obtained using TDDFT methodologies.[56] Optimal triplet state geometries needed to calculate triplet emission (phosphorescence) were obtained using the SCF DFT restricted to triplet spin configuration. We were able to converge to different triplet states by starting with appropriate initial guesses for the wave function before optimization, thus recovering ^{3}MLCT and Ru ^{3}d–d states (Fig. 2) analyzed in the previous studies.[29,30,57] Subsequently, geometry of ^{3}MLCT state relevant to experiment was used for calculations of phosphorescence energies. The latter were determined by two techniques: TDDFT framework and ΔSCF method.[44] TDDFT directly computes transition energy of the lowest triplet state at its geometry. ΔSCF method is based on the difference in total energies between self-consistent calculations of the ground and excited state electronic configurations, being singlet and triplet spin states in this work, respectively. Generally, both solutions are variational in the latter method. Consistency between ΔSCF and TDDFT results justifies the validity of both techniques and allows one to avoid possible pitfalls in the TDDFT methods related to appearance of spurious CT states.[58,59]

In order to analyze the nature of calculated singlet and triplet excited states, we performed an NTO analysis based on the calculated transition density matrices.[41] This method offers the most compact representation of the transition density between the ground and excited states in terms of an expansion into single-particle transitions (hole and electron states for each given excitation). Here we refer to the unoccupied and occupied NTOs as "electron" and "hole" transition orbitals, respectively. Note that NTOs are not the same as virtual and occupied MO pairs from the ground state calculations. TDDFT typically mixes several pairs of the ground state MOs due to correlation effects. All MOs and NTOs shown in this paper were produced with an orbital isovalue of 0.02 and visualized with GaussView 4.1 interface.[60]

Experimental

The metal complexes used in the experimental measurements were prepared by established literature procedures.[61] Complex **1**: the sample was purchased from Aldtrich as a chloride salt in form $[Ru(bpy)_3]Cl_2{\cdot}6H_2O$ (99.95% purity). The complex was converted to PF_6 salt *via* metathesis using saturated solution of NH_4PF_6 in water. No elemental analysis was performed following the metathesis. Complexes **2–4** were synthesized using literature procedure,[61] and the purity of the products were characterized by elemental analysis. For complex **2**, analysis calc. for $C_{32}H_{26}F_{12}N_6O_2P_2Ru$: C 41.89, H 2.86, N 9.16, found: C 41.71, H 2.86, N 8.89. For complex **3**, analysis calc. for $C_{34}H_{30}F_{12}N_6O_5P_2Ru$: C 41.10, H 3.04, N 8.46, found: C 40.83, H 2.95, N 8.78. For complex **4**: analysis calc. for $C_{96}H_{114}F_{24}N_{12}O_9P_4Ru_2$: C 48.82, H 4.86, N 7.12, found C 48.92, H 5.09, N 6.92.

For the optical measurements, the complexes were dissolved in acetonitrile (spectrophotometric grade, $\geq$ 99.5, Sigma-Aldrich). In order to protonate and deprotonate the carboxylic acid group on the bipyridine ligands, 1×10^{-5} M solution of the complex in acetonitrile was titrated dropwise with 1M HPF_6 or NaOH until no changes in absorption spectra have observed. Typically, addition of 20 μL of acid or base to 4 mL of complex solution ($\sim$500 fold molar excess) resulted in complete protonation or deprotonation of the complex, respectively.

The absorption spectra were collected on the Agilent 8453 UV-Visible Spectrophotometer in the absorbance mode. Steady state photoluminescence spectra were collected using Jobin-Yvon, Fluorolog-3 Fluorimeter, using 400 nm excitation wavelength in 1 cm quartz cuvettes, at room temperature. The spectra were corrected for the spectrometer response using correction factors provided by the manufacturer. The extinction coefficients of protonated and deprotonated forms of the

complexes **2–4** were determined by measurements of absorption spectra of the acetonitrile solutions with known complex concentrations, yielding the following values. Complex **1**: extinction coefficients ε(452 nm) = 14,500 ($\pm$300) cm^{-1} M^{-1}. Complex **2**: ε(458 nm) = 13,000 ($\pm$500) cm^{-1} M^{-1}; complex **2a**: ε(456) = 12,600 ($\pm$500) cm^{-1} M^{-1}. Complex **3**: ε(464 nm) = 9,000 ($\pm$500) $cm^{-1}M^{-1}$; complex **3a**: ε(462) = 8,800 ($\pm$500) cm^{-1} M^{-1}. Complex **4**: ε(494 nm) = 13 500 ($\pm$400) $cm^{-1}M^{-1}$; complex **4a**: ε(462 nm) = 18 000($\pm$500).

Results and discussion

Ground state analysis

We start with investigations of possible changes in the ground state electronic structure arising when fully protonated or deprotonated mcb or ccb groups are added to one or two bipyridine moieties. In Fig. 1, the Kohn–Sham energy diagram represents the ground state electronic structures of compounds **1–4** and their deprotonated analogues **2a–4a** in CH_3CN solvent. The three lowest unoccupied orbitals (LUMOs) and at least six highest occupied orbitals (HOMOs) of the functionalized complexes are compared to the unsubstituted complex **1**. Owing to the pseudo-octahedral coordination field of the bpy ligands, both the highest occupied and the lowest unoccupied MOs can be combined into groups of three.

Typical for Ru(II)-polypyridine complexes, the three highest occupied MOs have predominantly ruthenium d character (bonding t_{2g} states) with a small contribution from the nitrogen and carbon 2p character originating from the antibonding ligand orbitals in the complexes **1–4**. Because of the slight delocalization of their electron density to ligands, we denote these orbitals as t_{2g}-π^*. In the pristine complex **1**, the lower two states, HOMO-1 and HOMO-2, are degenerate with the energy by $\sim$0.16 eV smaller than the HOMO. In the complexes **2–4**, the distortions in the octahedral configuration brought by ligand functionalization break the degeneracy of HOMO-1 and HOMO-2 and split them by $\sim$30 meV. However, the splitting between these orbitals and the HOMO stays nearly the same as in the complex **1**. In addition to the degeneracy breaking, presence of carboxyl groups leads to a slight stabilization of the t_{2g}-π^* orbitals, compared to those in the complex **1**. Acting as weak electron acceptors, COOH-groups pull electron density from the nitrogen atoms in the bpy ligands, which results in a reduced repulsion between the nitrogen lone pairs and Ru(II) d-orbitals.

In contrast, the triad of t_{2g}-π^* orbitals is destabilized in the deprotonated complexes **2a–4a** because of the highly electron-rich character of the carboxylate ions. Surprisingly, the orbitals strongly localized on the COO^- groups with vanishing metal character have the highest energies and lie above and between t_{2g}-π^* states in the deprotonated compounds, as shown in Fig. 1. This result differs from the conclusions obtained for the tetradeprotonated thiocyanide-Ru complexes with Cl^- and NCS^- ligands,[23,24] where isolated orbitals with strong localization on the COO^-, Cl^-, and NCS^- ions lie significantly below t_{2g}-π^* orbitals. Compared to vacuum calculations, it is expected that solvent environment leads to stabilization of these localized states. Indeed, the quantitative behavior of these orbitals with respect to other occupied states depends on the solvation model used in calculations and the chemical compositions of ligands of Ru(II) complexes.

To clarify this question, we compare the electronic structures of deprotonated complexes **2a–4a** with geometries optimized in vacuum and in acetonitrile implementing different PCM solvation models available in Gaussian03 and Gaussian09. The results of this comparison are shown in Fig. 3. The relative energy position of localized COO^- orbitals with respect to the delocalized t_{2g}-π^* orbitals strongly depends on the solvation model and optimization procedure. For all deprotonated complexes, PCM-Gaussian03 solvent model stabilizes COO^- orbitals shifting them below t_{2g}-π^* triad for structures optimized in vacuum, Fig. 3(A). For the same vacuum geometries, CPCM-Gaussian03 solvent model provides analogous results (not shown). However, stabilization of COO^- orbitals decreases when the advanced solvent model based on PCM-Gaussian09 is used for the electronic structure calculations of vacuum geometries, Fig. 3(B). In this case, only one of three t_{2g}-π^* orbitals stays above the localized COO^- states. Optimization of geometries in acetonitrile using PCM-Gaussian09 results in the strong destabilization of COO^- orbitals shifting them to higher energies above (and between) t_{2g}-π^* orbitals, Fig. 3(B_1). Geometry optimization by PCM-Gaussian03 solvation model (A_1) also leads to destabilization of COO^- orbitals; however, destabilized COO^- orbitals are only slightly shifted above t_{2g}-π^* states. Overall, solvent simulations based on PCM-Gaussian09 model have a tendency of a stronger destabilization of the localized COO^- orbitals compared to PCM- or CPCM-Gaussian03 model.

Importantly, neither geometry optimization in vacuum or in solvent, nor the solvent model significantly affect positions of t_{2g}-π^* orbitals; their energies change only by 0.01–0.04 eV depending on the complex and the solvation model used. As we discuss in the next section, the Ru-centered t_{2g}-π^* orbitals contribute to the lower energy optically active transitions, while the contribution of COO^- orbitals to these transitions is negligible. Since the stabilization or destabilization of COO^- orbitals and its dependence on the solvation method does not affect lower-energy absorption spectra of deprotonated molecules **2a–4a**, discussion of COO^- orbitals is neglected in our further analysis of optical properties of these complexes.

Ligand functionalization and deprotonation strongly affect the lower-energy unoccupied orbitals. The three lowest unoccupied orbitals of all studied compounds have a π^* character and are delocalized over ligands . One of the major effects of the ligand carboxylation is the substantial stabilization of the LUMOs with respect to those of the complex **1**. For protonated compounds, this stabilization is stronger than stabilization of their HOMOs leading to the reduced HOMO–LUMO gap with respect to the pristine complex **1**. Stronger stabilization of the LUMO in the functionalized complexes originates from the change in its character (for details see Fig. S1 in ESI†). Thus, the LUMO is localized on the functionalized ligand(s) (mcb-π^* or ccb-π^* orbitals) in complexes **2–4**, compared to the delocalized character of the LUMO over all bpy ligands in the complex **1**. Neighboring lower-energy unoccupied orbitals in the functionalized complexes are localized on the unsubstituted bpy ligands

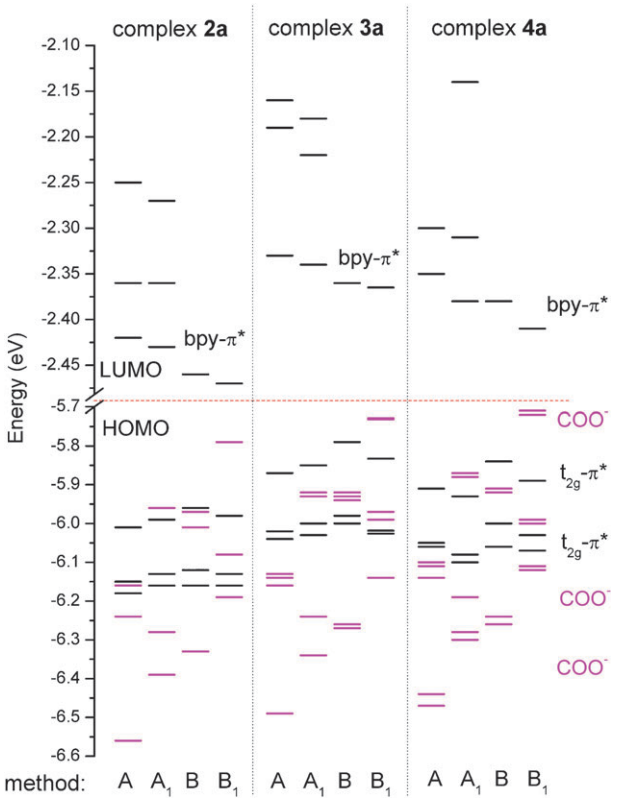

Fig. 3 Effect of solvation model on energies of the nearest to the gap occupied and unoccupied orbitals in the deprotonated complexes **2a–4a** on the solvation model. In method A and B, the geometries are optimized in vacuum, while the electronic structure is calculated in CH_3CN using PCM-Gaussian03 (A) or the advanced PCM-Gaussian09 (B) solvation models. In method A_1 and B_1 both the geometry optimization and the electronic structure are calculated in CH_3CN based on either PCM-Gaussian03 (A_1) or PCM-Gaussian09 (B_1) solvation models. Energies of the orbitals localized on the COO^- group strongly depend on the solvation model, while t_{2g}-π* orbitals are insignificantly affected. The effect of the solvation model on the LUMO (bpyπ*) is also very small compared to those on COO^- orbitals.

(bpy-π*-orbitals) and their energies are just slightly perturbed by the carboxyl groups (Fig. 1).

Deprotonation of the carboxyl groups, however, leads to the significant destabilization of the mcb-π* or ccb-π* orbitals due to the increased electron density on the COO^- ions. As a result, the energies of these orbitals lie above those of the non-substituted ligands. Therefore, for deprotonated compounds **2a–4a**, the LUMO has the bpy-π* character. Compared to the protonated complexes, bpy-π* orbitals are slightly destabilized (by ~0.1 eV) due to small contribution of electronic density delocalized over the ligands functionalized with carboxylate groups. Destabilization of the LUMO and change in its character in the deprotonated compounds lead to a small increase in the energy difference between the LUMO and the occupied t_{2g}-π* orbital, compared to those of protonated complexes **2–4**. Such a blue energy-shift caused by deprotonation agrees well with the previous results for the deprotonated thiocyanide-Ru(II) complex.[20,23,24]

It is important to note that both types of orbitals significantly contribute to optically allowed transitions in protonated and deprotonated complexes we study. Therefore, the increased energy separation between the ground state bpy-π* and t_{2g}-π* orbitals in the deprotonated complexes can be related to the observed blue shift in their absorption spectra. In addition, reordering of the unoccupied orbitals bpy-π* and mcb-π* or ccb-π* is reflected in the shape and width of the absorption spectra of the deprotonated compounds, which we discuss in the next section.

Analysis of absorption and emission spectra

The absorption spectra of the protonated and deprotonated compounds **2–4** calculated in acetonitrile solvent are shown in Fig. 4 and 5 and compared to the experimental data. The general trends in the absorption bands are very well reproduced by the theory, apart from a systematic (~0.25 eV) blue-shift of all theoretically predicted absorption energies. Such shift is a typical error for the TDDFT calculations.[32,43–46] In addition, the aforementioned lack of vibrational effects and the absence of counter ions in the calculations (providing potentially incomplete description of the solvent) could lead to such discrepancy. Nonetheless, the qualitative agreement between the theory and experiment is good enough to understand the nature of significant excited states in these systems.

In the visible region (Fig. 4), a strong absorption band is observed and accompanied by a pronounced shoulder for both protonated and deprotonated complexes. According to the accepted convention,[21,22,24] we denote these bands as I and II. The energies of the first two bright bands obtained by TDDFT and their comparison with the maxima in the experimental absorption spectra are summarized in Table 1. Based on our TDDFT NTOs analysis (Fig. 6 and 7) both bands can be characterized as the MLCT states. As illustrated in Fig. 6 and 7, optical excitations occur from the occupied (hole) transition orbitals to the unoccupied (electron) transition orbitals. Hole NTOs contributing to the bands I and II are mainly localized on the Ru center with a small portion of π* orbitals of ligands (t_{2g}-π*). The electron NTOs are mainly delocalized over either the π*-orbital of the bpy or the π*-orbital of the mcb or ccb ligands with a very small portion of electronic density on the Ru. As a result, there is a partial overlap between the electron and hole wavefunctions, which supports an oscillator strength of approximately 0.1–0.2 if allowed by the symmetry of the Ru d-orbitals and π*-orbitals of ligands. Typically, larger delocalization of the hole and electron NTOs over the Ru site and the ligands leads to increase in excited state transition dipole moment. Nonetheless, only a few MLCT transitions are optically allowed ("bright"); majority of MLCT excitations have very small (<0.06) oscillator strengths and are optically inactive ("dark"), including the lowest energy transition. Similar to MO arrangement, all MLCT transitions are aligned in triads, which is caused by the nearly triple degeneracy of the t_{2g}-π* hole NTOs, and by the octahedral environment of the ligands, as discussed previously.

Protonated functionalized complexes. In the protonated complexes **2–4**, the LUMO of ground state is stabilized, as discussed above (Fig. 1). This orbital strongly contributes to the lowest-energy bright excitations. In particular, the electron NTO involved in the bright excitations in the band I has the

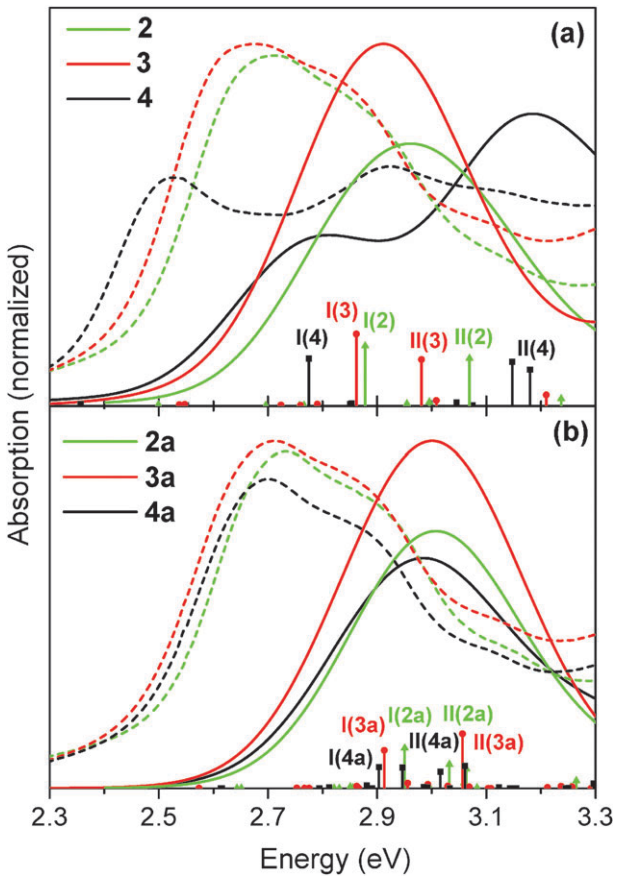

Fig. 4 Experimental and theoretical absorption spectra for the compounds **2–4**, with fully protonated carboxyl groups (a), and their fully deprotonated analogues **2a–4a** (b). Dash lines stay for experimental data; solid lines show calculated results. The oscillator strengths of calculated excited states are shown as vertical lines at the corresponding energies. I and II denote the lowest-energy and the higher-energy optically active bands I and II in the absorption spectra. Despite the uniform blue shift of ~0.25 eV, calculated spectra are in good qualitative agreement with experimental spectra.

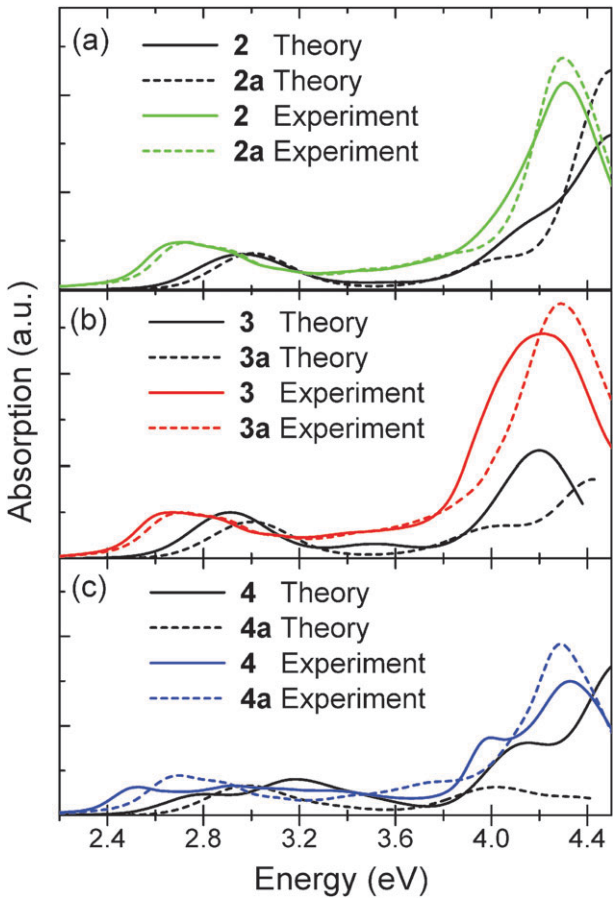

Fig. 5 Comparison of the calculated and experimental absorption spectra for protonated (solid line) and deprotonated (dashed line) complexes **2** (panel a), **3** (panel b) and **4** (panel c) in a wider energy region. For all complexes, deprotonation leads to a blueshift in the absorption spectrum.

dominant contribution of the LUMO for the complexes **2** and **4** and a combination of quasi-degenerate LUMO and LUMO + 1 for complex **3**. These ground state unoccupied orbitals are only slightly perturbed by electron correlation effects, as can be seen from the comparison of NTOs in Fig. 6 and the ground state MOs in Fig. S1–S2 in ESI.† Therefore, stabilization of the LUMO in compounds functionalized with carboxyl groups leads to a red-shift in the absorption maximum. As can be seen from Table 1, the magnitude of the red-shift for the band I increases from compound **1** to compound **4**, since LUMO of compound **4** is most effectively stabilized by the electron-withdrawing ccb group.

The character of the electron orbitals, *i.e.*, the type of the ligand on which the NTO involved in the optical transition is localized, controls the origin of the absorption bands I and II in the protonated complexes. Thus, the lower-energy excitation (band I) promotes the electron density to ligand(s) with the carboxyl substituent(s), *i.e.*, their LUMOs. In contrast, the second band (a shoulder at around 3 eV) in the absorption spectra of the protonated compounds involves the charge transfer from the Ru center (t_{2g}-π-orbitals) to the unsubstituted bpy ligands. Complexes **2** and **4** have two nearly degenerate electron orbitals localized on each of the unsubstituted bpy ligands. Therefore, the II-band excitations are described by contributions of two NTOs with a similar hole character, and an electron localized on each of the bpy ligands (only one of the NTO pairs are shown in Fig. 6). Since contributions from mcb and ccb groups are insignificant to the excitations in the band II for these compounds, they have very similar electron and hole NTO characters, and identical transition energies. However, for compound **3**, the resulting electron wavefunction includes also some portion of the lower lying mcb-π*-orbitals, which leads to the stabilization of the excitation and decrease in the transition energy (Table 1).

Another interesting issue is the separation between the two low-energy bands, which is responsible for the shape and width of the absorption spectrum in Fig. 4(a). We found that the energy difference between absorption bands I and II is directly related to the energy splitting between the ground state orbitals localized on the unsubstituted ligands (bpy-π*) and orbitals localized on the functionalized ligands (mcb-π* or ccb-π*). For the complex **4**, this splitting is significantly larger, because the ccb-π*-orbital (LUMO) is stabilized much

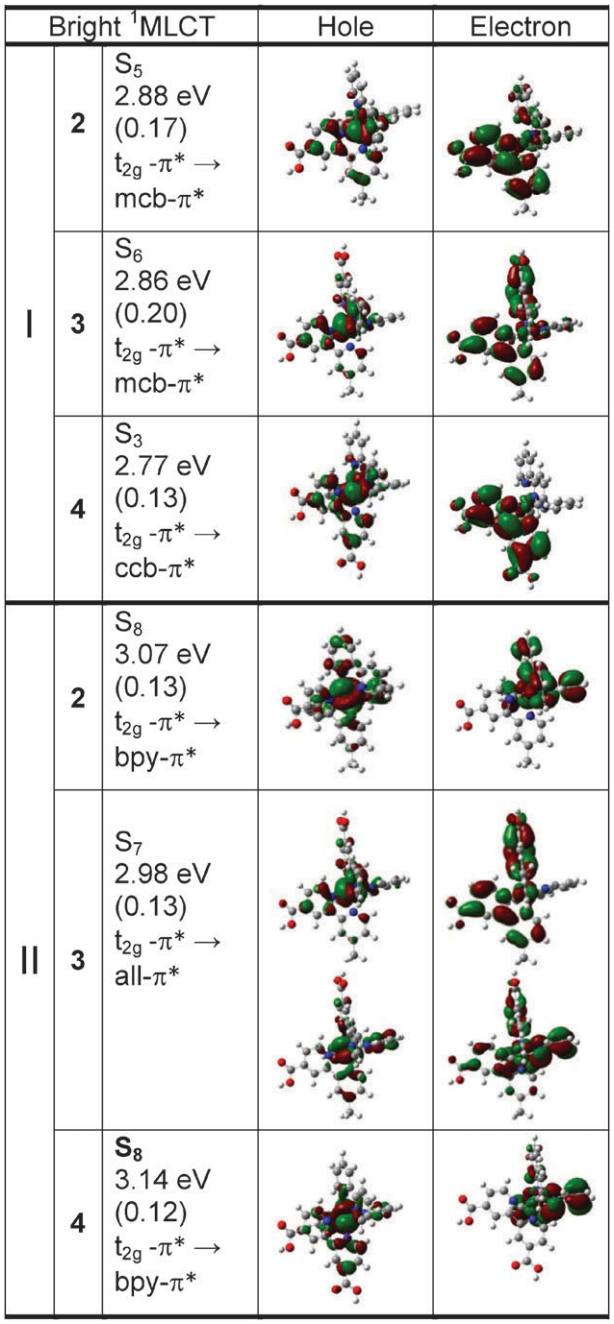

Fig. 6 Natural transition orbitals (NTOs) for the complexes **2**, **3**, and **4** illustrating the nature of optically active singlet excited states in the absorption bands I and II. For each state, the respective number of the state, the transition energy (eV), and the oscillator strength (in parentheses) are listed. Shown are only occupied (holes) and unoccupied (electrons) NTO pairs that contribute more than 30% to each excited state. All transitions are MLCT in character: the charge is transferred from the Ru t_{2g}-π* hole orbital to the ligands with the COOH-group(s) (mcb-π* or ccb-π* electron orbital) in the lowest-energy band I, or to the bpy-ligands (bpy-π*) in the higher-energy band II.

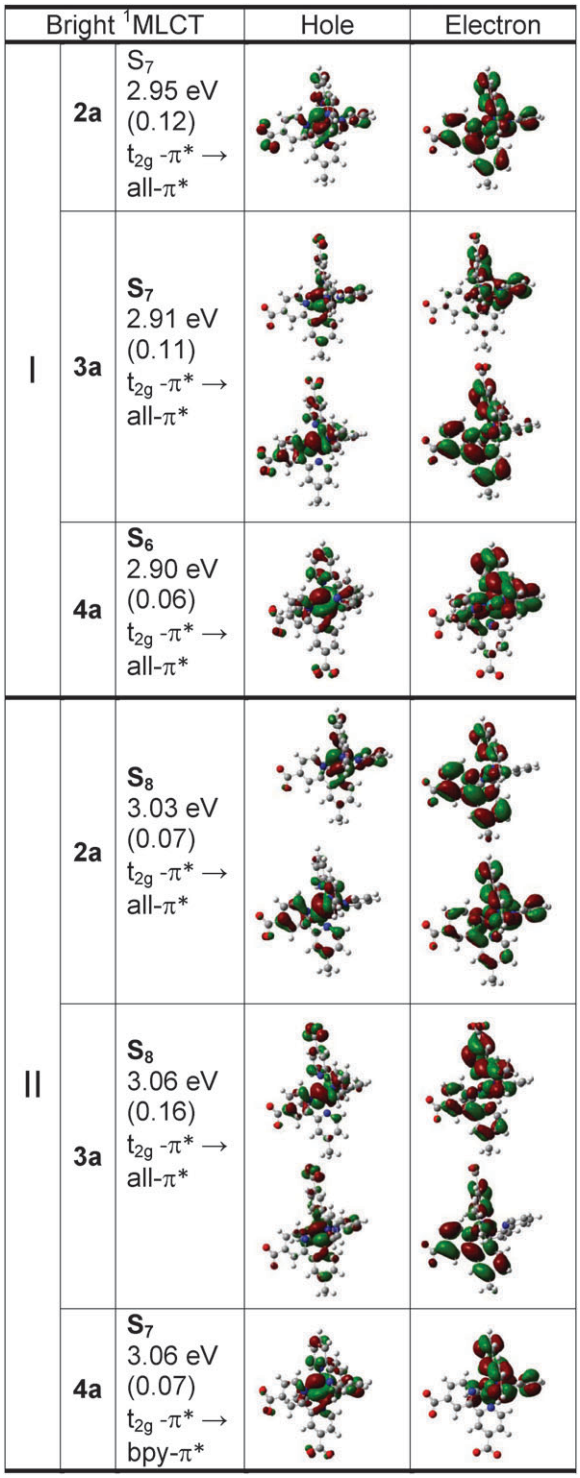

Fig. 7 Natural transition orbitals (NTOs) for deprotonated complexes **2a–4a** illustrating the nature of the optically active singlet excited states in the absorption bands I and II. The oscillator strength of each transition is listed in parentheses below its transition energy (eV). Shown are only occupied (holes) and unoccupied (electrons) NTO pairs that contribute more than 30% to each excited state. Similar to the protonated complexes, all transitions are MLCT in character; however, the electron transition orbitals are substantially delocalized over all ligands.

stronger when two COOH groups are present on the same bpy ligand, compared to the compounds **2** and **3**. Theoretically predicted increase in splitting between bands I and II for the complex **4** is in a good agreement with experimental data (Fig. 4a). However, the band splitting, a well-recognized shoulder in Fig. 4a, is more pronounced in experimental

Table 1 Experimental and theoretical absorption and photoluminescence (PL) data for all Ru-complexes we studied. E^E_{PL} corresponds to the maxima in the experimental PL-spectra; E^E_{abs} corresponds to the maxima in the experimental absorption spectra. E^T_{abs-I} and E^T_{abs-II} correspond to the first and second optically allowed excited states with the oscillator strength >0.07 calculated with TDDFT method (roughly corresponding to the maxima of bands I and II). E^T_{fl} is the singlet fluorescence transition calculated as a vertical transition between the lowest optimized excited and ground states, E^{T1}_{ph} and E^{T2}_{ph} are the vertical triplet transition energies (phosphorescence) calculated by the TDDFT and ΔSCF methods, respectively. These transition energies are schematically shown in Fig. 2

	Experiment		TDDFT				ΔSCF
Complex	E^E_{abs}	E^E_{PL}	E^T_{abs-I}	$E_{abs-II}{}^T$	E^T_{fl}	E^{T1}_{ph}	E^{T2}_{ph}
1	2.73	2.00	3.04	3.04	2.72	2.02	2.03
2	2.68	1.86	2.88	3.07	2.12	1.86	1.86
2a	2.70	1.97	2.95	3.03	2.21	1.97	2.17
3	2.64	1.84	2.86	2.98	2.17	1.86	1.86
3a	2.68	1.90	2.91	3.06	2.15	1.92	1.91
4	2.49	1.75	2.77	3.14	2.04	1.78	1.99
4a	2.66	1.97	2.90	3.06	2.19	1.95	1.94

spectra of complexes **2** and **3** than in the theoretical. Since this shoulder is present even in the experimental spectrum of the complex **1** (not shown), its origin is likely attributed to the vibrational overtones[62] often seen in the linear absorbance of organic chromophores. Other broadening mechanisms, such as spin–spin and spin–orbit couplings, which are not included in our calculations, might also contribute to the linewidths of the experimental spectra.[63]

Effect of deprotonation

A major effect of COOH deprotonation observed experimentally is a persistent blue-shift of absorption and photoluminescence (PL) maxima compared to that in the respective protonated complexes, as presented in Fig. 5 and Table 1. For example, difference in absorption peaks (E_{abs}) between protonated and deprotonated complexes **4** and **4a** is ~0.2 eV. This blue shift is well reproduced in our TDDFT calculations and agrees well with the previous studies of deprotonated Ru(II)thiocianyde-derivatives.[24] Analysis of NTOs and MOs for deprotonated species (Fig. 7 and S1, S2 in ESI†) clarifies the origin of such blue shift in absorption maxima. In analogy to the non-deprotonated complexes, the lowest-energy bright excitations in bands I and II involve MLCT transitions from the Ru-center (t_{2g}-π*-orbitals) to the ligand π*-orbitals. However, transitions in the deprotonated compounds are, in general, more delocalized and less structured than those in the protonated species. Such delocalization of electron NTOs leads to decreased energy splitting between bands I and II in the deprotonated compounds, which is the most pronounced in the complex **4a**, Fig. 4b.

Subsequently, this electronic delocalization strongly affects the static dipole moment magnitudes in the ground and excited states. These quantities summarized in Table 2 have been calculated for the ground state singlet and MLCT triplet state geometries. In all protonated compounds, excited state dipole moments are nearly twice as large as their ground state counterparts for both ground state absorption (compare μ_0 and μ_S) and triplet state emission (compare μ'_0 and μ'_T). The situation is opposite in the deprotonated compounds: Coulomb interactions between positive charge on Ru and negative charges on one or two ligands significantly increase the dipole moments compared to that of parent protonated complexes. However, because of the MLCT character of singlet and triplet states, there is a decrease of the static dipole moment of deprotonated molecules in their excited states. This change in the dipole moment is reflected in the more delocalized character of electron NTOs (Fig. 7) for excited state transitions, when compared to the analogous transitions in the protonated complexes (Fig. 6). Thus, in agreement with previous studies,[22] negative solvatochromism is expected for the deprotonated complexes, because their ground state dipole moments are larger than the excited state ones (see Table 2). This contrasts conventional positive solvatochromism in the protonated molecules, where the opposite trend is conformed for their ground and excited state dipoles. Consequently, deprotonation leads to blue shifts in both experimental and calculated absorption and emission spectra. The larger difference between the static dipole moment of the ground and excited states of the deprotonated molecule would lead to an increased blue-shift of the absorption maxima. For example, in the complex **4a**, two COO^- groups are located on the same bpy ligand increasing its dipole moment up to $\mu_0 \sim 21$ Debye, compared to the complex **2a** with a single COO^- group ($\mu_0 \sim 13$ Debye) and the complex **3a** with two COO^- groups that are separated form each other on different bpy ligands ($\mu_0 \sim 16$ Debye). However, the static excited-state dipole moments are roughly the same ($\mu_S \sim$ 12–14 Debye) for all deprotonated compounds (Table 2). Therefore, the blue shift in the absorption energy is more significant for the complex **4a**.

For both protonated and deprotonated complexes, next bright highly intense peak is observed in the near-UV energy region of ~4.2 eV, as presented in Fig. 5. It arises from the intraligand π–π* transitions and gains its intensity from the increased density of excited states in related energy region. Compared to the MLCT bands I and II, the position and the shape of this peak is more affected by the deprotonation of the carboxyl substituent, because it is completely dominated by ligand-localized electron and hole NTOs, including orbitals localized on the COO^- groups. Note that this peak has a smaller blue shift (<0.2 eV) with respect to experimental data, compared to the first peak originating from MLCT (0.25–0.3 eV). Such inconsistency of the theoretical prediction of energies for two main absorption peaks relative to the experimental data is

Table 2 Static dipole moments (in Debye) for the lowest singlet ^{1}MLCT and triplet ^{3}MLCT states. These quantities are calculated at ground state geometry, absorption point (ground μ_0 and lowest singlet excited state μ_S), and ^{3}MLCT state geometry, phosphorescence point (ground μ'_0 and lowest triplet excited state μ'_T)

	Ground state		^{3}MLCT	
Complex	μ_0	μ_S	μ'_0	μ'_T
2	6.52	13.30	7.17	17.31
2a	13.43	11.87	12.91	10.94
3	8.50	15.40	8.24	16.32
3a	16.15	13.56	15.70	13.64
4	10.66	18.06	10.27	14.47
4a	20.58	13.83	20.50	18.98

likely related to a different nature of the excited states: π–π* intraligand excitations and MLCT transitions, the latter being particularly problematic for TDDFT theory.

Emission spectra

Experimental and theoretical absorption and emission energies (see Fig. 2 for notations) of the Ru-complexes studied here are listed in Table 1. In experiments, the emission energies (E^E_{PL}) are about 0.7–0.8 eV smaller than the energy of the first absorption peak (E^E_{abs}) for all complexes. This difference is not a conventional vibrational Stokes shift, since emission of Ru-complexes is expected to originate from the low-energy triplet state (phosphorescence), rather than from the excited singlet state. Optically forbidden nature of the lowest excited state and spin–orbit coupling facilitate the intersystem crossing into a weakly-allowed triplet state lying below the bright singlet states.[36] Our theoretical results support experimental data. Indeed, calculated vertical singlet fluorescence energies (E^T_{fl}) for compounds **1–4** and their deprotonated analogues are lower by ~0.3–0.7 eV than their correspondent vertical absorption energies E^T_{abs-I} due to excited state vibrational relaxation, which can be very significant in organometalic complexes.[64] However, they are still notably higher than the experimental photoluminescence energies.

The calculated vertical phosphorescence energies using TDDFT (E^{T1}_{ph}) and ΔSCF (E^{T2}_{ph}) techniques[43,44] (as described above in the section on theoretical methodology) agree very well with each other and essentially reproduce experimental numbers E^E_{PL} for all compounds (Table 1). Hence application of both TDDFT and ΔSCF methods for studies of emission properties in Ru-complexes is justified and produces quantitative results. All calculated triplet states responsible for phosporescence are MLCT in character (^{3}MLCT). For the protonated species, the lowest energy ^{3}MLCT states look very similar to singlet MLCT (^{1}MLCT) transitions. In particular, in complexes **2–4**, an electron is promoted from the Ru(d) orbital to the ligand(s) functionalized with the COOH groups (Fig. 6). For the deprotonated complexes **2a** and **3a**, however, the electron NTO for the ^{3}MLCT excitation is localized on unsubstituted bpy-ligands with no admixture of the mcb-ligands (Fig. 7). Deprotonation of complexes **2–3** leads to the blue shift in phosphorescence energies, compared to those of their protonated analogous; although, this shift is slightly larger than in the case of absorption. This originates from the positive (negative) solvatochromism observed in the protonated (deprotonated) complexes as discussed in the previous section.

Another observation important for future TDDFT calculations of similar Ru-complexes, is complexity of their excited state potential energy surfaces.[39] We have found that the triplet state geometry optimization strongly depends on the initial guess. A good example of this effect is an interplay between the lowest ^{3}MLCT state and the triplet Ru ligand field d–d transition (^{3}d–d), Fig. 2. Thus, for ground state optimized geometry, the vertical ^{3}d–d transitions lie more than 3 eV above the ground state; therefore they can not contribute to phosphorescence. However, relaxation of the triplet excited state geometry can lead to the decrease of the Ru ^{3}d–d transition energy and results in the lowest triplet state of the Ru d–d-type, which lies about 1.2 eV above the ground singlet state. Representative transition orbitals and an energy level diagram for such scenario are shown in Fig. 8. A decrease in the transition energy of the ^{3}d–d vertical excitation arises from a slight decrease in the energy of the optimized triplet state and a large increase in the reference ground singlet state energy for the corresponding geometry.

Similar effects for the Ru-polypyridines were recently reported by Batista *et al.*[29,57] These studies have shown that the character of the lowest triplet excited state changes from ^{3}MLCT to ^{3}π–π* or ^{3}d–d, depending on the solvent polarity and initial guess for the triplet state in the Ru-terPy complex. Indeed, it was shown that the nature of the lowest triplet state and the emission energy depend on a variety of experimental conditions (solvent polarity, pH, counterions, ligand structure, *etc.*)[36–38] In our case, by choosing an appropriate initial guess, we obtained triplet state geometries corresponding either to the ^{3}d–d excitations with the small transition energies of about 1 eV or the ^{3}MLCT-type excited states with the transition energies of about 1.8–1.9 eV for all protonated and deprotonated complexes. Consequently, the choice of the initial electronic structure configuration has important implications for analysis of triplet states in the Ru-polypyridine complexes when using DFT-based quantum chemistry methods.

Conclusions

We studied in detail ground and excited state electronic structure of a family of Ru(II)-bipyridine complexes functionalized with carboxyl groups. We specifically focused on the changes in electronic structure and optical properties of these molecules caused by introducing the carboxyl groups onto the bpy ligands and deprotonation of these groups.

We have found that functionalization of the complexes with carboxyl groups differently affects the occupied and unoccupied electronic levels near the HOMO–LUMO gap in the complexes **2–4**. The HOMOs, which are Ru d (t_{2g}-π*) in character are not significantly affected by functionalization. In contrast, energies of the LUMOs, localized on the substituted ligands (mcb-π* or ccb-π* orbitals), are very strongly stabilized by the electron-withdrawing mcb or ccb groups. Consequently, functionalization of Ru(II)-bipyridine complexes with carboxyl groups insignificantly affects their ionization energies, while strongly increases their electron affinities. The decrease in the ground state HOMO–LUMO gap introduced by carboxyl groups is reflected in the redshifts of the absorption and emission spectra of complexes **2–4**. The TDDFT transition orbital analysis demonstrated that the lowest-energy bright transition has MLCT character promoting an electron from the t_{2g}-π* (HOMO) to the π*-orbital of the ligands (LUMO). Therefore, the redshift observed in the optical spectra is predominantly due to a strong stabilization of the LUMO (mcb-π* or ccb-π* electron transition orbitals).

In contrast, deprotonation of the functionalized ligands in the complexes **2–4** results in a blue-shift of the absorption and phosphorescence spectra compared to the parent compounds. This observation agrees with previous studies on related compounds.[22–24,31,32,39] This effect is rationalized by interplay

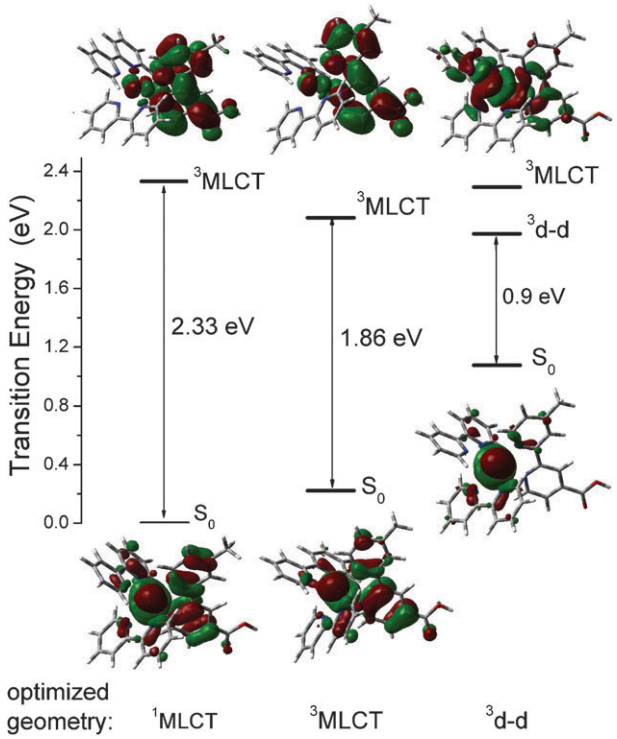

Fig. 8 Natural transition orbitals and energy level diagram for the complex **2** illustrating the nature of the lowest-energy triplet transition and its dependence on the initial geometry configuration. For the singlet MLCT state optimized in its ground state configuration (^{1}MLCT), the ^{3}MLCT transition is much lower than ^{3}d–d transition, which is more than 3 eV above the ground state and not shown. Relaxation of the triplet MLCT state in its excited state geometry (^{3}MLCT) significantly decreases the energy of ^{3}MLCT transition, while ^{3}d–d stays at 3.05 eV above the ground state (not shown). Triplet state geometries corresponding to the ^{3}d–d excitations provide the lowest ^{3}d–d transition energy.

of positive and negative solvatochromism in the protonated and deprotonated complexes, respectively, *i.e.*, calculated static dipole moments increase (decrease) in the excited states of protonated (deprotonated) complexes, leading to a different amount of solvent stabilization in ground and excited states.[22]

The lowest singlet and triplet states contributing to fluorescence and phosphorescence, respectively, are MLCT in character for both protonated and deprotonated complexes. The calculated transition energies for the triplet ^{3}MLCT states agree well with the experimental PL data. However, the character of the calculated lowest triplet excited state can change from the optically allowed ^{3}MLCT to the optically forbidden ^{3}d–d transitions, depending on the initial guess of the triplet configuration. Such strong dependence of the triplet state optimization on the initial guess is attributed to the complexity of the excited state potential energy surfaces that leads to the close proximity and change in relative positions of the Ru d-levels and the π-levels of the ligands, as has been also observed in other Ru(II) complexes.[29,30] Theoretically predicted interplay between the lowest ^{3}MLCT and the Ru ^{3}d–d transitions suggests that the efficiency of the triplet emission in these molecules can be quite sensitive to experimental conditions. Finally, for the ground state calculations of deprotonated compounds **2a–4a**, we found that in contrast to the t_{2g}-π* orbitals, the energies of occupied orbitals localized on COO^- group(s) strongly depend on the solvation model used in calculations. However, the localized COO^- orbitals do not contribute to the optical transitions and do not affect absorption and emission in the MLCT region.

Overall, the presented studies establish applicability of DFT and TDDFT methods to analyze excited states, absorption and emission properties of Ru-compounds. Our results for the functionalized protonated and deprotonated molecules can be useful to better understand and optimize applications of such molecules in photo-electro-chemical cells and catalyst agents based on TiO_2/Ru-complex[15,65] and quantum dot/Ru-complex materials.[16]

Acknowledgements

The authors are grateful to Richard L. Martin, Enrique R. Batista, and Sergei Ivanov for their generous and insightful advice on TDDFT simulations. VA thanks Dmitri Kilin for his gracious support and fruitful discussions regarding the physical properties of metal complexes and semiconductor nanostructures. This work was supported by the US Department of Energy and Los Alamos LDRD funds. Los Alamos National Laboratory is operated by Los Alamos National Security, LLC, for the National Nuclear Security Administration of the US Department of Energy under contract DE-AC52-06NA25396. We acknowledge the support of the Center for Integrated Nanotechnology (CINT) and the Center for Nonlinear Studies (CNLS).

References

1 T. J. Meyer and M. H. V. Huynh, *Inorg. Chem.*, 2003, **42**, 8140–8160.
2 M. H. V. Huynh, D. M. Dattelbaum and T. J. Meyer, *Coord. Chem. Rev.*, 2005, **249**, 457–481.
3 T. R. Prytkova, I. V. Kurnikov and D. N. Beratan, *Science*, 2007, **315**, 622–625.
4 J. H. Alstrum-Acevedo, M. K. Brennaman and T. J. Meyer, *Inorg. Chem.*, 2005, **44**, 6802–6827.
5 V. Balzani, G. Bergamini, F. Marchioni and P. Ceroni, *Coord. Chem. Rev.*, 2006, **250**, 1254–1266.
6 F. G. Gao and A. J. Bard, *J. Am. Chem. Soc.*, 2000, **122**, 7426–7427.
7 L. Zhang and S. Dong, *Anal. Chem.*, 2006, **78**, 5119–5123.
8 K. E. Erkkila, D. T. Odom and J. K. Barton, *Chem. Rev.*, 1999, **99**, 2777–2796.
9 Q. Wang, S. M. Zakeeruddin, M. K. Nazeeruddin, R. Humphry-Baker and M. Grätzel, *J. Am. Chem. Soc.*, 2006, **128**, 4446–4452.
10 K. Tennakone, G. Kumara, I. Kottegoda, K. Wijayantha and V. Perera, *J. Phys. D: Appl. Phys.*, 1998, **31**, 1492–1496.
11 H. Zabri, I. Gillaizeau, C. A. Bignozzi, S. Caramori, M. Charlot, J. Cano-Boquera and F. Odobel, *Inorg. Chem.*, 2003, **42**, 6655–6666.
12 M. Grätzel, *Nature*, 2001, **414**, 338–344.
13 D. Kuang, C. Klein, Z. Zhang, S. Ito, J.-E. Moser, S. M. Zakeeruddin and M. Grätzel, *Small*, 2007, **3**, 2094–2102.
14 J. A. Treadway, J. A. Moss and T. J. Meyer, *Inorg. Chem.*, 1999, **38**, 4386–4387.
15 L. Gallagher, S. Serron, X. Wen, B. Hornstein, D. Dattelbaum, J. Schoonover and T. J. Meyer, *Inorg. Chem.*, 2005, **44**, 2089–2097.
16 M. Sykora, M. A. Petruska, J. Alstrum-Acevedo, I. Bezel, T. J. Meyer and V. I. Klimov, *J. Am. Chem. Soc.*, 2006, **128**, 9984.
17 C. Klein, M. K. Nazeeruddin, D. D. Censo, P. Liska and M. Grätzel, *Inorg. Chem.*, 2004, **43**, 4216–4226.

18 N. Nickita, M. J. Belousoff, A. I. Bhattt, A. M. Bond, G. B. Deacon, G. Gasser and L. Spiccia, *Inorg. Chem.*, 2007, **46**, 8638–8651.
19 L. G. C. Rego and V. S. Batista, *J. Am. Chem. Soc.*, 2003, **125**, 7989–7997.
20 L. Fodor, G. Lendvay and A. Horvath, *J. Phys. Chem. A*, 2007, **111**, 12891–12900.
21 M. Nazeeruddin, F. De Angelis, S. Fantacci, A. Selloni, G. Viscardi, P. Liska, S. Ito, B. Takeru and M. Grätzel, *J. Am. Chem. Soc.*, 2005, **127**, 16835–16847.
22 S. Fantacci, F. De Angelis and A. Selloni, *J. Am. Chem. Soc.*, 2003, **125**, 4381–4387.
23 F. D. Angelis, S. Fantacci, A. Selloni and M. K. Nazeeruddin, *Chem. Phys. Lett.*, 2005, **415**, 115–120.
24 F. D. Angelis, S. Fantacci and A. Selloni, *Chem. Phys. Lett.*, 2004, **389**, 204–208.
25 M. K. Nazeeruddin, A. Kay, I. Rodicio, R. Humphry-Baker, E. Mueller, P. Liska, N. Vlachopoulos and M. Grätzel, *J. Am. Chem. Soc.*, 1993, **115**, 6382–6390.
26 M. T. Indelli, M. Ghirotti, A. Prodi, C. Chiorboli, F. Scandola, N. D. McClenaghan, F. Puntoriero and S. Campagna, *Inorg. Chem.*, 2003, **42**, 5489.
27 C. Goze, C. Sabatini, A. Barbieri, F. Barigelletti and R. Ziessel, *Eur. J. Inorg. Chem.*, 2008, 1293–1299.
28 F. Schramm, V. Meded, H. Fliegl, K. Fink, O. Fuhr, Z. Qu, W. Klopper, S. Finn, T. E. Keyes and M. Ruben, *Inorg. Chem.*, 2009, **48**, 5677–5684.
29 E. R. Batista and R. L. Martin, *J. Phys. Chem. A*, 2005, **109**, 9856–9859.
30 M.-F. Charlot and A. Aukauloo, *J. Phys. Chem. A*, 2007, **111**, 11661–11672.
31 M. Charlot, Y. Pellegrin, A. Quaranta, W. Leibl and A. Aukauloo, *Chem.–Eur. J.*, 2006, **12**, 796–812.
32 J. E. Monat, J. H. Rodriguez and J. K. McCusker, *J. Phys. Chem. A*, 2002, **106**, 7399–7406.
33 X. Yang and M.-H. Baik, *J. Am. Chem. Soc.*, 2008, **130**, 16231–16240.
34 G. B. Shaw and J. M. Papanikolas, *J. Phys. Chem. B*, 2002, **106**, 6156–6162.
35 J. R. Schoonover, D. M. Dattelbaum, A. Malko, V. I. Klimov, T. J. Meyer, D. J. Styers-Barnett, E. Z. Gannon, J. C. Granger, W. S. Aldridge and J. M. Papanikolas, *J. Phys. Chem. A*, 2005, **109**, 2472–2475.
36 R. S. Lumpkin, E. M. Kober, L. A. Worl, Z. Murtaza and T. J. Meyer, *J. Phys. Chem.*, 1990, **94**, 239–243.
37 M. Sykora and J. R. Kincaid, *Inorg. Chem.*, 1995, **34**, 5852–5856.
38 M. K. Brennaman, T. J. Meyer and J. M. Papanikolas, *J. Phys. Chem. A*, 2004, **108**, 9938–9944.
39 J. K. McCusker, *Acc. Chem. Res.*, 2003, **36**, 876–887.
40 M. J. Frisch, *et al.*, *GAUSSIAN 09*, Gaussian, Inc., Wallingford, CT, 2009.
41 R. L. Martin, *J. Chem. Phys.*, 2003, **118**, 4775.
42 R. G. Parr and W. Yang, *Density-Functional Theory of Atoms and Molecules*, Oxford University Press, New York, 1989.
43 E. R. Batista and R. L. Martin, *J. Am. Chem. Soc.*, 2007, **129**, 7224–7225.
44 E. R. Batista and R. L. Martin, *J. Phys. Chem. A*, 2005, **109**, 3128–3133.
45 S. R. Stoyanov, J. M. Villegas and D. P. Rillema, *Inorg. Chem.*, 2002, **41**, 2941–2945.
46 J.-F. Guillemoles, V. Barone, L. Joubert and C. Adamo, *J. Phys. Chem. A*, 2002, **106**, 11354–11360.
47 V. N. Nemykin, R. G. Hadt, R. V. Belosludov, H. Mizuseki and Y. Kawazoe, *J. Phys. Chem. A*, 2007, **111**, 12901–12913.
48 E. Jakubikova, W. Chen, D. M. Dattelbaum, F. N. Rein, R. C. Rocha, R. L. Martin and E. R. Batista, *Inorg. Chem.*, 2009, **48**, 10720.
49 J. Rusanova, E. Rusanov, S. I. Gorelsky, D. Christendat, R. Popescu, A. A. Farah, R. Beaulac, C. Reber and A. B. P. Lever, *Inorg. Chem.*, 2006, **45**, 6246–6262.
50 S. I. Gorelsky, S. C. da Silva, A. Lever and D. W. Franco, *Inorg. Chim. Acta*, 2000, **300–302**, 698 708.
51 C. J. Cramer and D. G. Truhlar, *Phys. Chem. Chem. Phys.*, 2009, **11**, 10757–10816.
52 S. F. Sousa, P. A. Fernandes and M. J. Ramos, *J. Phys. Chem. A*, 2007, **111**, 10439–10452.
53 V. Barone, M. Cossi and J. Tomasi, *J. Comput. Chem.*, 1998, **19**, 404–417.
54 M. Cossi, N. Rega, G. Scalmani and V. Barone, *J. Comput. Chem.*, 2003, **24**, 669–681.
55 D. M. York and M. Karplus, *J. Phys. Chem. A*, 1999, **103**, 11060–79.
56 F. Furche and R. Ahlrichs, *J. Chem. Phys.*, 2002, **117**, 7433–7447.
57 E. Jakubikova, W. Chen, D. M. Dattelbaum, F. N. Rein, R. C. Rocha, R. L. Martin and E. R. Batista, *Inorg. Chem.*, 2009, **48**, 10720–10725.
58 R. Magyar and S. Tretiak, *J. Chem. Theory Comput.*, 2007, **3**, 976–987.
59 A. Dreuw and M. Head-Gordon, *J. Am. Chem. Soc.*, 2004, **126**, 4007–4016.
60 R. Dennington-II, T. Keith and J. Millam, *GaussView, Version 4.1*, Semichem, Inc., Shawnee Mission, KS, 2007.
61 B. M. Peek, G. T. Ross, S. W. Edwards, G. J. Meyer, T. J. Meyer and B. W. Erickson, *Int. J. Pept. Protein Res.*, 1991, **38**, 114–123.
62 O. S. Odongo, M. J. Heeg, Y.-J. Chen, P. Xie and J. F. Endicott, *Inorg. Chem.*, 2008, **47**, 7493–7511.
63 E. M. Kober and T. J. Meyer, *Inorg. Chem.*, 1982, **21**, 3967–3977.
64 P. Sinha, A. K. Wilson and M. A. Omary, *J. Am. Chem. Soc.*, 2005, **127**, 12488–12489.
65 J. Huang, D. Stockwell, Z. Huang, D. L. Mohler and T. Lian, *J. Am. Chem. Soc.*, 2008, **130**, 5632–5633.